The Drift of Midocean Jets

DORON NOF AND W. K. DEWAR*

Department of Oceanography and Geophysical Fluid Dynamics Institute, The Florida State University, Tallahassee, Florida

(Manuscript received 18 May 1992, in final form 8 December 1992)

ABSTRACT

The migration of nonlinear frontal jets is examined using an inviscid "reduced gravity" model. Two cases are considered in detail. The first involves the drift of deep jets situated above a sloping bottom, and the second addresses the zonal β-induced migration of meridional jets in the upper ocean. Both kinds of jets are shallower on their left-hand side looking downstream (in the Northern Hemisphere). For the first case, *exact* nonlinear analytical solutions are derived, and for the second, two different methods are used to calculate the approximate migration speed.

It is found that deep oceanic jets migrate along isobaths (with the shallow ocean on their right-hand side) at a speed of $g'S/f_0$ (where g' is the reduced gravity, S the slope of the bottom, and f_0 the Coriolis parameter). This speed is *universal* in the sense that all jets migrate at the same rate regardless of their details. By contrast, upper-ocean meridional jets on a β plane drift westward at a speed that *depends on their structure.* Specifically, it is shown that this drift is the average of the two long planetary wave speeds on either side of the front: namely, $C = -\beta(R_{d+}^2 + R_{d-}^2)/2$, where $R_{d+}(R_{d-})$ is the deformation radius based on the undisturbed depth east (west) of the jet; for frontal jets the above formula gives half the long Rossby wave speed.

Both kinds of drift occur even if the jets in question are slanted; that is, it is not necessary that the deep jets be directly oriented uphill (or downhill) or that the upper-ocean jets be oriented in the north–south direction. For the drifts to exist, it is sufficient that the deep jets have an uphill (or downhill) component and that the β-plane jets have a north–south component. Possible application of this theory to the jet observed during the Local Dynamic Experiment, which has been observed to drift westward, is discussed.

1. Introduction

The question of what happens to meridional midocean jets on a β plane or deep jets situated over a sloping bottom is important because of its direct relevance to jets in the open ocean. One example of such flows is the midocean jet discovered during the Local Dynamic Experiment (Shen et al. 1986). This jet was observed to have a relatively short cross-front length scale (50–100 km) and an alongfront length scale of at least 400 km. It was a surface intensified feature, with flows at 200 m in excess of 30 cm s^{-1} and cross-front isopycnal depth changes of ~200 m. Last, the jet appeared to be associated with a considerable mass transport. These aspects of the Local Dynamics Experiment (LDE) jet suggest that it is an important feature of the North Atlantic circulation.

Past theoretical models of the LDE jet, and of midocean jets in general, have examined possible reasons for their existence, but have confined their analysis to time-independent fixed processes (Dewar 1991; Dewar and Marshall 1993). An observed feature of the LDE jet, however, was its tendency to move west at a rate of a few centimeters per second and the reasons for such migration have received only limited study. The objective of this paper, therefore, is to examine propagating front models that can, hopefully, be applied to the LDE observations.

Background

It has been recognized for many years that upper-ocean features with *closed* circulation cells (i.e., Rossby waves or eddies) propagate to the west on a β plane and that similar deep patterns migrate along isobaths. However, it is not a priori obvious what would be the case with *one-dimensional meridional* flows because the common qualitative explanations for the westward drift of Rossby waves (e.g., Gill 1982) and eddies (e.g., Nof 1983a) do not apply. This is so because both of these explanations rely on the presence of *zonal* flows that are not necessarily present in meridional jets.

A partial answer to the question of the behavior of meridional β-plane fronts was obtained in a study of planetary shock waves in Dewar (1987). There it was argued (using a two-layer model) that steepening, driven by the nonlinearity in the continuity equation

* Also affiliated: Supercomputer Computations Research Institute.

Corresponding author address: Prof. Doron Nof, Department of Oceanography 3048, The Florida State University, Tallahassee, FL 32306-3048.

in the presence of β, produced westward migration of the front. These same planetary shock wave dynamics accounted for front generation in the steady arrested fronts model described by Dewar (1991). Although useful, the above is limited in that the flow was everywhere restricted to being geostrophic, even in the main body of the jet. A ramification of pure geostrophy, however, is that the well-known Sverdrup constraint governs net transport, so that the strong upper-layer jet flows are accompanied by reverse deep flows that very nearly cancel the total volume flux. In contrast, the LDE jet observations suggest that the jet flows were surface intensified, but in the same southwesterly direction *throughout* the water column. Furthermore, transport estimates suggested that the jet was moving 40 Sv of the fluid to the southwest, which is greatly out of accord with Sverdrup dynamics.

In view of this, it is of interest to examine a broader class of midocean jets than has previously been considered and to determine how they respond to the presence of β. To do so, we shall look at two inviscid jets—a heavy deep f-plane jet situated over a sloping bottom and a light upper-ocean jet on a β plane. The deep jet is examined first (section 2) because its analysis is considerably simpler than that of the upper jet. By examining the flow in a coordinate system traveling with the jet at its own migration speed, an exact analytical solution is derived. It shows that the migration is caused by the gravitational force that forces the jet downhill. This force is, in turn, balanced by a Coriolis force that corresponds to an along-isobath drift.

With the aid of this exact solution for the deep-ocean jet, we shall then examine upper-ocean jets (section 3). Here, it is impossible to derive an exact analytical solution. However, by integrating the y-momentum equation and using a perturbation in ϵ, the ratio of the variation of the Coriolis parameter across a segment of the jet to the Coriolis parameter at the center, it is possible to derive an approximate solution for a meridional jet with vanishing thickness on one side. It is also possible to obtain an approximation to the front drift speed in the more general cases of (i) differing, but not necessarily vanishing, thicknesses on each side of the front and (ii) nonmeridional fronts. After presenting these analytical solutions, we present a possible application of the model to the jet observed during the LDE (section 4). The results are discussed and summarized in section 5.

2. Deep jets over a sloping bottom

a. Formulation

As an idealized formulation of the problem, consider the jet shown in Fig. 1. The cold homogeneous jet has a density $(\rho + \Delta\rho)$, depth $h(x, y)$, and horizontal velocity components $u = u(x, y)$ and $v = v(x, y)$. The infinitely thick fluid above has a density (ρ) and is taken to be at rest.

When there is no slope to the bottom ($S \equiv 0$), the jet is obviously stationary ($C_x \equiv 0$) and has the familiar structure:

$$\left.\begin{aligned} v &= (g'H)^{1/2}e^{-x/Rd}, \quad u = 0 \\ h &= H(1 - e^{-x/Rd}) \end{aligned}\right\} \quad \textit{uphill jet (i.e., jet occupying the area } x \geq 0\textit{)} \tag{2.1a}$$

$$\left.\begin{aligned} v &= -(g'H)^{1/2}e^{x/Rd}, \quad u = 0 \\ h &= H(1 - e^{x/Rd}) \end{aligned}\right\} \quad \textit{downhill jet (i.e., jet occupying the area } x \leq 0\textit{),} \tag{2.1b}$$

where the jets' potential vorticity $[\partial v/\partial x + f_0]/h$ is uniform (f_0/H), H is the undisturbed depth at infinity, R_d, the deformation radius, equals $(g'H)^{1/2}/f_0$, g' is the "reduced gravity," $(\Delta\rho/\rho)g$, and f_0 is the (uniform) Coriolis parameter. The above relationships describe a jet that is in a geostrophic balance in the x direction (i.e., $f_0 v = g'\partial h/\partial x$) and does not vary in y (i.e., $\partial/\partial y \equiv 0$).

With the aid of this information, we shall now examine the more general problem of a jet over a sloping bottom (i.e., $S \neq 0$). To do so, we shall consider a coordinate system traveling with the jet at its yet unknown migration speed C_x. The origin of the coordinate system is located along the front ($h = 0$), the x axis is directed at 90° to the left of the downhill direc-

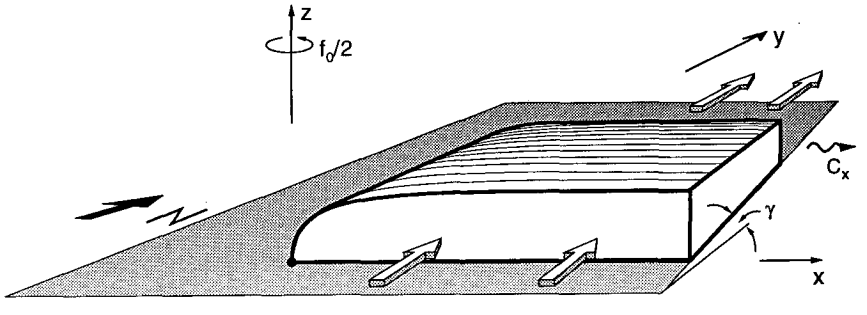

FIG. 1a. Three-dimensional view of the reduced-gravity deep-ocean jet under study. The "wavy" arrow indicates migration and straight arrows correspond to actual flows. The bottom slope is defined by $S \equiv \tan\gamma$.

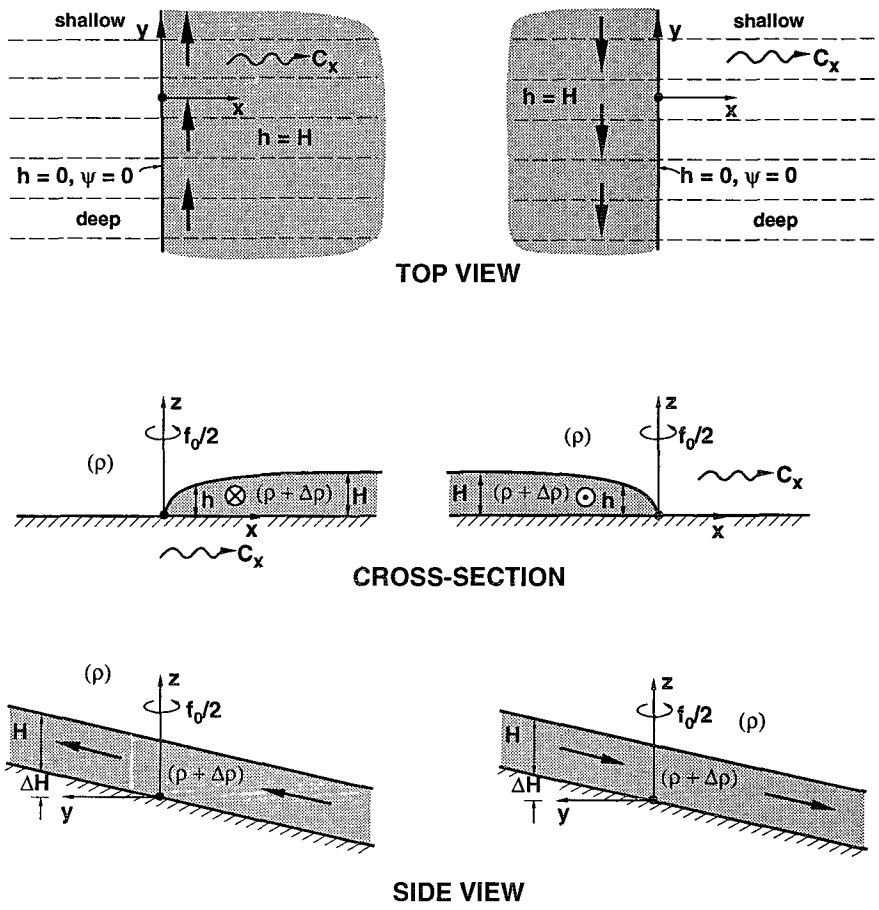

FIG. 1b. Schematic diagram of the reduced-gravity deep-ocean jet under study. Thick arrows denote flow direction and "wavy" arrows denote migration; dashed lines denote isobaths. The bottom slope corresponds to $\Delta H - Sy$. The jet is flowing either uphill (left panel) or downhill (right panel) and migrates along the isobaths (i.e., in a direction perpendicular to the flow direction).

tion, the y axis is pointed uphill, and, as before, the system rotates uniformly with an angular velocity $f_0/2$ about the vertical axis.

It is assumed that the translation is steady and that the shape of the jet does not change in time so that in our moving coordinate system the motion appears to be steady. The assumption of permanent form and structure is plausible, but it is not a priori obvious under what conditions it is valid and adequate. It will be demonstrated later, however, that the drift does not affect the structure of the jet in any way so that the shape is indeed permanent, and the assumption is adequate for all topographically induced drifts.

The relevant governing equations for the moving coordinate system (x, y) are obtained by applying the transformations $\hat{x} \to x + C_x t$ and $\hat{y} \to y$ to the familiar equations in the fixed system $(\hat{x}, \hat{y})$. For the conditions mentioned above, the transformed equations are

$$u\frac{\partial u}{\partial x} + v\frac{\partial u}{\partial y} - f_0 v = -\frac{1}{\rho}\frac{\partial P}{\partial x} \qquad (2.2)$$

$$u\frac{\partial v}{\partial x} + v\frac{\partial v}{\partial y} + f_0(u + C_x) = -\frac{1}{\rho}\frac{\partial P}{\partial y} \qquad (2.3)$$

$$\frac{\partial}{\partial x}(hu) + \frac{\partial}{\partial y}(hv) = 0, \qquad (2.4)$$

where P is the deviation of the hydrostatic pressure from the hydrostatic pressure associated with a state of rest (i.e., a "no jet" state), and $f_0 C_x$ is an apparent Coriolis force resulting from the fact that our coordinate system is moving.

Under these conditions, P can be expressed as

$$P = g\Delta\rho[h(x, y) + Sy - z], \qquad (2.5)$$

where S is the slope of the bottom. Substitution of (2.5) into (2.2) and (2.3) gives the modified equations,

$$u\frac{\partial u}{\partial x} + v\frac{\partial u}{\partial y} - f_0 v = -g'\frac{\partial h}{\partial x} \qquad (2.6)$$

$$u\frac{\partial v}{\partial x} + v\frac{\partial v}{\partial y} + f_0(u + C_x + g'S/f_0) = -g'\frac{\partial h}{\partial y}, \qquad (2.7)$$

which are subject to the boundary conditions,

$$h = 0; \quad \psi(x, y) = 0 \tag{2.8a}$$

$$v \to 0; \quad x \to \pm\infty, \tag{2.8b}$$

where ψ, the transport function, is defined by

$$\frac{\partial \psi}{\partial x} = vh; \quad \frac{\partial \psi}{\partial y} = -uh. \tag{2.9}$$

Condition (2.8a) states that the jet is bounded by a front ($h = 0$) whose structure and shape are not known in advance but rather must be found as a part of the problem. Condition (2.8b) reflects the fact that the jet's speed decays away from the front; the plus and minus signs correspond to uphill and downhill jets, respectively.

b. Solution

Examination of (2.6)–(2.7) reveals that if C_x is set to be equal to $-g'S/f_0$ then the governing shallow-water equations reduce to the *same* form that they would have in the absence of any slope. This implies, of course, that they admit the exact jet solution discussed earlier in (2.1). Hence, the exact solution for our drifting jet is

$$\boxed{C_x = -g'S/f_0}$$
$$v = (g'H)^{1/2}e^{-x/Rd}; \quad u = 0$$
$$h = H(1 - e^{-x/Rd})$$
$$\Big\} \quad \text{uphill jet (i.e., } \infty > x \geq 0; \; -\infty < y < \infty) \tag{2.10a}$$

or

$$\boxed{C_x = -g'S/f_0}$$
$$v = -(g'H)^{1/2}e^{-x/Rd}; \quad u = 0$$
$$h = H(1 - e^{x/Rd})$$
$$\Big\} \quad \text{downhill jet (i.e., } -\infty < x \leq 0; \; -\infty < y < \infty), \tag{2.10b}$$

where u, v are now the speeds as viewed from the *moving* coordinate system.

At this point, the reader may wonder how particles can move uphill (downhill) without losing (gaining) energy. This apparent conflict is resolved by examining the Bernoulli integral in the moving system,

$$\frac{1}{2}(u^2 + v^2) + g'h + g'Sy + f_0C_xy = B(\psi). \tag{2.11b}$$

In this form, the Bernoulli incorporates both the slope and the drift; since $C_x = -g'S/f_0$, the last two terms drop out and we recover the usual Bernoulli implying that the uphill (downhill) motions are offset by the general drift. This results from the fact that the gravitational force, $g'S$, is balanced by the Coriolis force associated with the drift, f_0C_x, so that particles are free to move up and down the slope without losing or gaining energy. Note also that our solution requires, of course, that at infinity the fluid will actually be moving at the same rate that the front migrates. In contrast to the meridional upper-ocean jet that will be later described in section 3, the present bottom jet does not vary in the y direction. Here, the exact solution illustrates that, although the slope causes a drift, it has no influence on the jet's structure.

It is important to point out that our jet's general drift is identical to the migration speed at which isolated cold eddies drift (Nof 1983b; Mory 1985; Mory et al. 1987). This universal speed, sometimes referred to as the Nof speed (e.g., Swaters and Flierl 1991), corresponds to an identical balance of forces (gravitational and Coriolis) and, hence, it is not surprising that the speeds are also identical.

c. Slanted jets

We shall now show that the above solution for the drift (2.10) is also applicable to jets whose orientation does not coincide with the downhill direction (Fig. 2). For such jets the governing shallow-water equations (2.6)–(2.7) are rewritten in the form,

$$\tilde{u}\frac{\partial \tilde{u}}{\partial \tilde{x}} + \tilde{v}\frac{\partial \tilde{u}}{\partial \tilde{v}} - f_0\left(\tilde{v} + C_{\tilde{y}} + \frac{g'S\cos\alpha}{f_0}\right) = -g'\frac{\partial h}{\partial \tilde{x}} \tag{2.12}$$

$$\tilde{u}\frac{\partial \tilde{v}}{\partial \tilde{x}} + \tilde{v}\frac{\partial \tilde{v}}{\partial \tilde{y}} + f_0\left(\tilde{u} + C_{\tilde{x}} + \frac{g'S\sin\alpha}{f_0}\right) = -g'\frac{\partial h}{\partial \tilde{y}}, \tag{2.13}$$

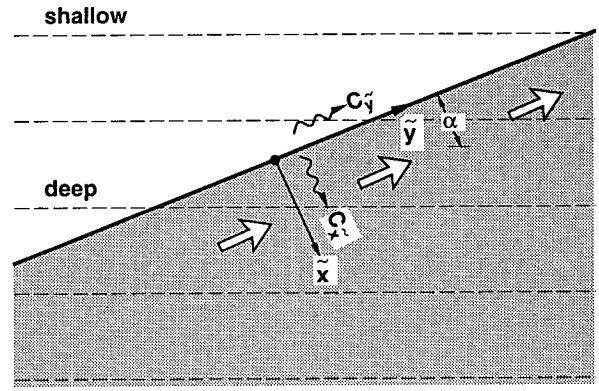

TOP VIEW

FIG. 2. The same as Fig. 1 but for a slanted jet, that is, instead of flowing directly uphill or downhill, the jet is now flowing at an angle α (measured from a line parallel to the isobaths to the front), which is smaller than $\pi/2$. $C_{\tilde{x}}$ and $C_{\tilde{y}}$ are the drifts in the $\tilde{x}$ and $\tilde{y}$ directions of the new tilted (and moving) coordinate system.

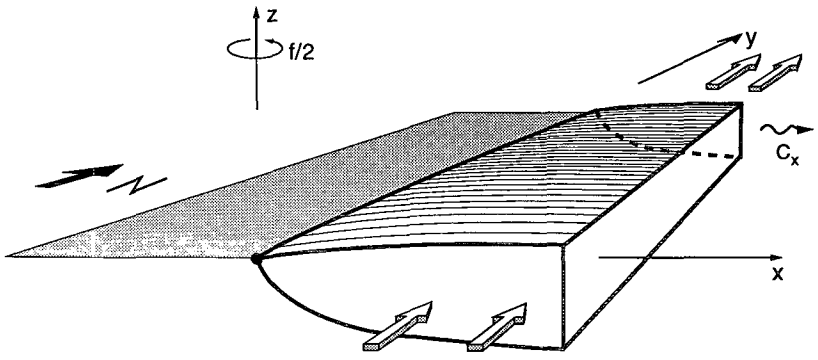

FIG. 3a. A three-dimensional view of a reduced-gravity upper-ocean jet on a β plane.

where the tildes represent the new coordinate system; that is, $\tilde{u}$ and $\tilde{v}$ are the velocity components in the slanted (and traveling) coordinate system (Fig. 2). Note that for $\alpha = \pi/2$, (2.12) and (2.13) reduce to (2.6) and (2.7) as should, of course, be the case.

By setting $C_{\tilde{y}} = -(g'S/f_0)\cos\alpha$ and $C_{\tilde{x}} = -(g'S/f_0)\sin\alpha$ [which corresponds to $C = -(C_{\tilde{y}}^2 + C_{\tilde{x}}^2)^{1/2} = -g'S/f_0$] we again recover the usual shallow-water equations on a flat bottom. This indicates that, as in the $\alpha = \pi/2$ case (i.e., uphill jet), the jet is not affected by the drift so that its structure and form are identical to that described by (2.1). In view of this, we conclude that all deep jets, regardless of their orientation, migrate "westward" (i.e., with shallow water to the right) at the *universal* speed $g'S/f_0$.

3. Upper-ocean jets

With the aid of the exact solution for the cold deep jets over a sloping bottom, we shall now discuss upper-ocean jets on a β plane. Before doing so it is appropriate to point out that, for the case under discussion, the analogy between a sloping bottom and β is only *qualitative* in nature (i.e., the direction of propagation for an eddy on a β plane and an eddy on a sloping bottom is expected to be identical but the specific values of the drifts are expected to be quite different). This is so because the classical *quantitative* analogy is due to conservation of potential vorticity associated with stretched columns of fluid, which change their depth as the fluid moves across the slope. In contrast, the depth of our deep oceanic jets is not directly affected by the slope. That is to say, the only effect of the slope is to introduce a gravitational component to the governing equations so that the classical analogy does not apply in a quantitative manner.

We present two different approaches to the analysis of front drift. The first assumes the presence of an essentially meridional jet. This assumption is not necessary for the second approach; however, less detailed information about the jet structure emerges from the second approach than the first.

a. *First formulation*

Consider the northward flowing frontal jet shown in Fig. 3. As before, we begin by looking at the governing equations in a moving coordinate system assuming that, in such a system, the jet appears to be steady,

$$u\frac{\partial u}{\partial x} + v\frac{\partial u}{\partial y} - (f_0 + \beta y)v = -g'\frac{\partial h}{\partial x} \quad (3.1)$$

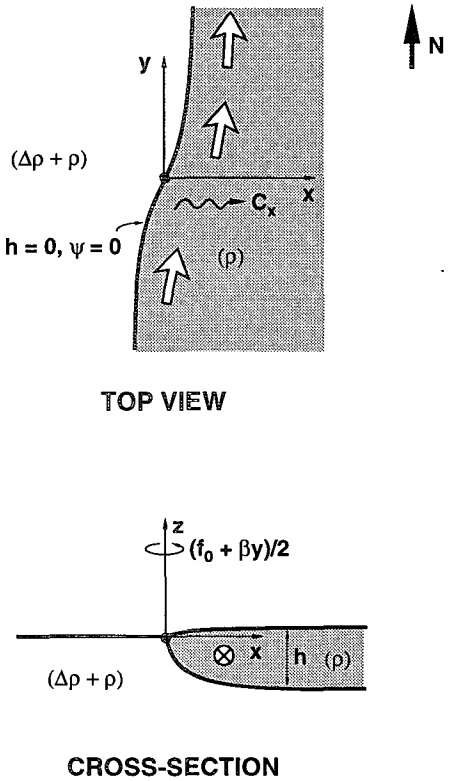

FIG. 3b. Schematic diagram of the upper-ocean jet under study. The jet is oriented mainly in the north–south direction and can be flowing either northward or southward (not shown). Namely, due to β, it varies slowly with y but rapidly with x so that the deviations of the front from a pure meridional orientation are $\sim R_d$.

$$u\frac{\partial v}{\partial x} + v\frac{\partial v}{\partial y} + (f_0 + \beta y)(u + C_x) = -g'\frac{\partial h}{\partial y} \quad (3.2)$$

$$\frac{\partial}{\partial x}(hu) + \frac{\partial}{\partial y}(hv) = 0. \quad (3.3)$$

It is further assumed that the jet is *varying slowly with y* and is in a cross-stream geostrophic balance; that is, the length scale in the y direction, L, is much greater than the scale in the x direction [which is, of course, the deformation radius $R_d \equiv (g'H)^{1/2}/f_0$] and $v \gg u$ so that the flow is mainly northward. Under such conditions, (3.2) and (3.3) remain unaltered but (3.1) can be approximated by

$$(f_0 + \beta y)v = g'\frac{\partial h}{\partial x}. \quad (3.4)$$

Note that the slowly varying structure in y was not present in the bottom jets discussed earlier in section 2 because the sloping bottom had no effect on the jet's f-plane structure. As expected, when $\beta = 0$, the equations possess a solution of a *stationary* jet whose structure is identical to that of the flat-bottom jet (2.1a). For both the f-plane case ($\beta \equiv 0$) and the full problem ($\beta \neq 0$), the boundary conditions are identical to those of the bottom jet, that is,

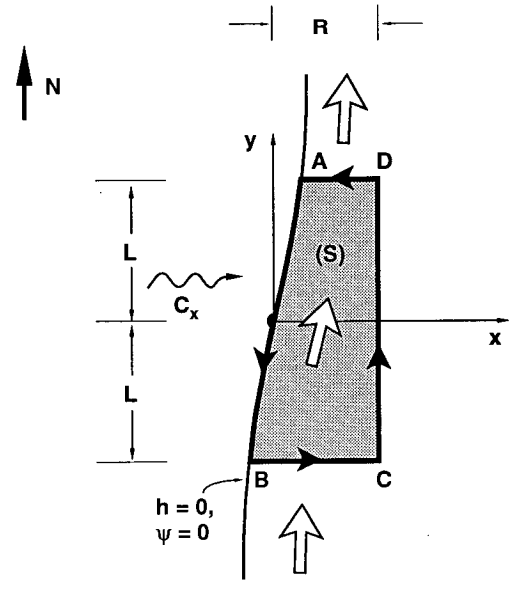

FIG. 4a. The integration area of the frontal jet shown in Fig. 3. Section DC is situated well beyond the jet's decay area (i.e., at least several deformation radii away from the front). Sections AD and BC are situated a distance L (much greater than the Rossby radius, R_d, but much smaller than the radius of the earth, a) away from the x axis. It is assumed that the meridional flow is geostrophic in cross sections AD and BC. Also, since the front is drifting, entrainment or detrainment (i.e., $u \neq 0$) is allowed at infinity ($x \to \infty$) even though $v \to 0$.

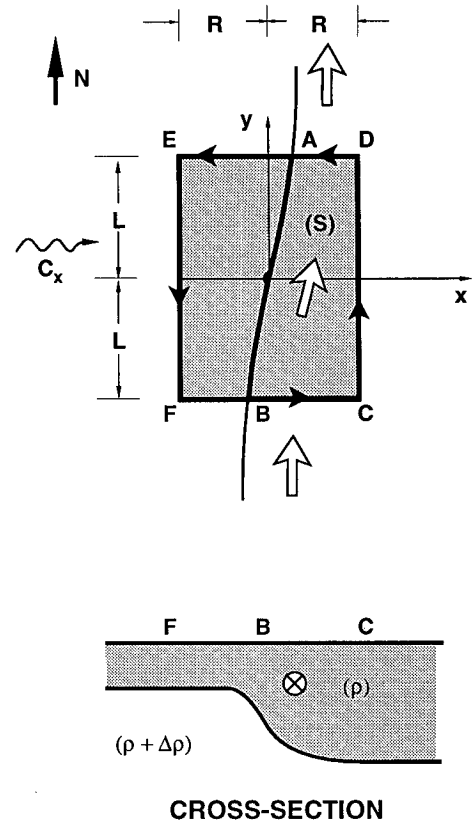

FIG. 4b. The integration area of the meridional nonfrontal jet (upper panel). As before, sections DC and EF are situated well beyond the jet's decay area (i.e., at least several deformation radii away from the front). A cross section of the jet's structure upstream is shown in the lower panel.

$$h = 0; \quad \psi(x, y) = 0 \quad (3.5a)$$

$$v \to 0; \quad x \to \infty. \quad (3.5b)$$

b. Solution

In this subsection the general solution will be derived.

1) INTEGRATED MOMENTUM EQUATION

To obtain the solution, (3.2) is multiplied by h and integrated over the area shown in Fig. 4, to give

$$\iint_S \left(hu\frac{\partial v}{\partial x} + hv\frac{\partial v}{\partial y}\right)dxdy + \iint_S (f_0 + \beta y)(u + C_x)hdxdy + \frac{g'}{2}\iint_S \frac{\partial}{\partial y}(h^2)dxdy = 0, \quad (3.6)$$

which, by using the continuity equation (3.3), can be reduced to

$$\iint_S \left[\frac{\partial}{\partial x}(huv) + \frac{\partial}{\partial y}(hv^2)\right]dxdy$$

$$- \iint_S (f_0 + \beta y)\frac{\partial \psi}{\partial y}\,dxdy + \iint_S f_0 C_x h dxdy$$

$$+ \frac{g'}{2}\iint_S \frac{\partial}{\partial y}(h^2)dxdy = 0. \quad (3.7)$$

Application of Stokes' theorem to (3.7) gives,

$$\oint_\phi huvdy - \oint_\phi (hv^2 + g'h^2/2)dx$$

$$- \iint_S f_0 \frac{\partial \psi}{\partial y}\,dxdy + \iint_S f_0 C_x h dxdy$$

$$- \beta \iint_S \left[\frac{\partial}{\partial y}(y\psi) - \psi\right]dxdy = 0, \quad (3.8)$$

where ϕ is the boundary of S and the arrowed circles indicate counterclockwise integration. Before proceeding, it is recalled that the meridional flow is geostrophic along AD and BC and that, since the jet is drifting, an entrainment or detrainment (i.e., $u \neq 0$) is allowed as $x \to \infty$ (i.e., along DC). Note, however, that $v \to 0$ as $x \to \infty$ because the jet decays away from the front. Since at least one of the three variables h, u, and v vanishes on every portion of the boundary ϕ, (3.8) can be rearranged and written as,

$$\oint_\phi [hv^2 + g'h^2/2 - (f_0 + \beta y)\psi]dx$$

$$+ f_0 \iint_S C_x h dxdy + \beta \iint_S \psi dxdy = 0. \quad (3.9)$$

We now note that (3.4) can be multiplied by h and integrated once in x to give,

$$(f_0 + \beta y)\psi = g'h^2/2 + C, \quad (3.10)$$

where the integration constant C must be zero because $\psi = 0$ where $h = 0$ (i.e., along the front). In view of (3.10), (3.9) can be approximated by

$$\oint_\phi hv^2 dx + f_0 \iint_S C_x h dxdy + \beta \iint_S \psi dxdy = 0, \quad (3.11)$$

where the first term represents the flow force associated with the mass flux of the jet, the second is the force due to the drift, and the third is the flow force due to β. The scales of the parameters appearing in (3.11) are as follows: within the core of the jet,

$$v \sim O[(g'H)^{1/2}];\ \psi \sim O(g'H^2/f);\ C \sim O(\beta R_d^2)$$

$$y \sim O(L);\quad x \sim O(R_d);\quad u \sim O\left[\frac{R_d}{L}(g'H)^{1/2}\right],$$

whereas outside the jet's core (i.e., $x > R_d$),

$$v, u \sim O(\beta R_d^2),\quad C \sim O(\beta R_d^2).$$

This scaling takes into account that the jet is varying slowly in the y direction and that there could be both zonal and meridional entrainment of $O(\beta R d^2)$.

Since v decays to $O(\beta R d^2)$ away from the front, the first term becomes relatively small (compared to the other two) as the integration area is increased by increasing R (see Fig. 4). Namely, when $R \to \infty$, (3.11) gives,

$$\boxed{f_0 \iint_S C_x h dxdy + \beta \iint_S \psi dxdy = 0};\quad R \to \infty, \quad (3.12)$$

where the ratio of the neglected integral [i.e., the first term in (3.11)] to the terms that are kept is $\sim O(\beta R_d/f_0)(R_d/L)$, which is typically 10^{-3} or even smaller.

2) Scaling and expansions

We proceed by scaling C_x with βR_d^2, x with R_d, y with L, h with H, and ψ with $g'H^2/f_0$, which together with (3.12) give

$$C_x^* \iint_{S^*} h^* dx^* dy^* + \iint_{S^*} \psi^* dx^* dy^* = 0. \quad (3.13)$$

Note that $R_d \ll L \ll a$ where a is the radius of the earth [$O(f_0/\beta)$]. That is to say, L is a length scale in between the radius of the earth and the deformation. For convenience we shall later take L to be the so-called intermediate length scale, but this is not really essential.

Next, h^*, ψ^*, and C_x^* are expanded in a power series in $\epsilon = \beta L/f_0$,

$$\left.\begin{aligned} h^*(x, y, \epsilon) &= h^{(0)}(x, y) + \epsilon h^{(1)}(x, y) + \cdots \\ \psi^*(x, y, \epsilon) &= \psi^{(0)}(x, y) + \epsilon \psi^{(1)}(x, y) + \cdots \\ C_x^* &= C_x^{(1)} + \epsilon C_x^{(2)} + \cdots \end{aligned}\right\}, \quad (3.14)$$

where $\epsilon \ll 1$ since $R_d \ll L \leqslant a$ (here, a is the radius of the earth). Note that the above scaling is consistent with values found for the LDE jet. Typical values for this jet are $R_d \sim 30$ km, while L, though not determined by the observations, might be taken as a few hundred kilometers, so that ϵ is typically $<O(0.1)$.

Our zeroth-order state ($\beta \equiv 0$, $h^{(0)}$, $\psi^{(0)}$) corresponds to a nondrifting frontal jet on an f plane and, as mentioned, the solution for such a jet (with a uniform potential vorticity) is given by (2.1). By substituting

(3.14) in (3.13) and collecting terms of order unity [$O(\epsilon^0)$] we obtain the *first-order* approximation,

$$C_x^{(1)} = -\iint \psi^{(0)} dx^* dy^* \Big/ \iint h^{(0)} dx^* dy^* . \tag{3.15}$$

This relationship *shows that, to first order, the drift is only a function of the zeroth-order jet* [i.e., the *f*-plane solution (2.1)]. Far away from the front ($R \to \infty$), the *f*-plane solution (2.1) gives $h^{(0)} \to 1$ and $\psi^{(0)} \to 1/2$ so that $C_x^{(1)} = -1/2$ and the final dimensional first-order drift is

$$C_x = -\beta R_d^2/2. \tag{3.16}$$

Three comments should be made with regard to our first-order solution (3.15)–(3.16). First, it is straightforward to show that for nonfrontal meridional jets (i.e., jets whose depth at $x < 0$ is not zero) the drift can be obtained by using the integration area shown in Fig. 4b. By repeating the procedures mentioned earlier and taking the limit as $R \to \infty$, one finds

$$C_x = \frac{-\beta g'(H_+ + H_-)}{2f_0^2} = \frac{-\beta(R_{d+}^2 + R_{d-}^2)}{2}, \tag{3.16b}$$

where H_+ and H_- are the undisturbed depths at $x \to \pm\infty$.

The second comment that should be made with regard to (3.16) is that we have not found the complete first-order solution, $\psi^{(1)}$, $h^{(1)}$. This implies that (i) we cannot say what is the corresponding entrainment or detrainment at $x \to \infty$ and (ii) we have not really proven that our solution is correct because the complete first-order solution may involve compatibility conditions that could, perhaps, be more restrictive than our scalings. While this is no doubt a weakness, it is very difficult—and probably impossible—to overcome because it is not at all clear that the most general first-order solution can ever be found analytically.

Third, note that the jet's *y* structure does not enter our first-order computation because of the particular structure of the integrated momentum equation. Namely, the integrated momentum states that the first-order migration speed is only a function of the local zeroth- ($\beta = 0$) order structure that does not vary in *y*.

c. *Second formulation*

It is also possible to use a somewhat different approach to show that (3.16b) is valid not only for meridional jets but also for slanted jets [in which an O(1) deviation from a purely meridional flow is allowed]. We shall briefly outline the approach here and describe the details in appendix A. In contrast to the previous approach, the present approach will not involve a rigorous perturbation scheme; instead, it is based solely on scaling and integration.

1) Governing equations

We consider the shallow water equation in a coordinate frame fixed to the earth:

$$\frac{\partial \mathbf{u}}{\partial t} + \mathbf{u}\cdot\nabla\mathbf{u} + f\mathbf{k}\times\mathbf{u} = -g'\nabla h \tag{3.17a}$$

$$\frac{\partial h}{\partial t} + \nabla\cdot(h\mathbf{u}) = 0, \tag{3.17b}$$

where boldface indicates vectors and the remaining notation is standard. We will now examine the constraints that (3.17) place on the behavior of a jet inclined at an arbitrary angle θ with respect to north (see Fig. 5). Recall that the width of the jet is of the order of the deformation radius, R_d. For convenience, we assume that the length scales of the water masses on either side of the front are basin scale [$O(f_0/\beta)$].

2) Integration

We begin by solving (3.17a) for the mass transport, which yields:

$$\mathbf{u}h = -\frac{1}{f}\nabla\times\frac{g'h^2}{2}\mathbf{k} + \mathbf{k}\times\frac{\partial(h\mathbf{u})/\partial t}{f} + \frac{\mathbf{F}}{f} \tag{3.18a}$$

where,

$$\mathbf{F} = \left[\frac{-\partial(uvh)}{\partial x}\frac{-\partial(vvh)}{\partial y}, \frac{\partial(uuh)}{\partial x}\frac{+\partial(uvh)}{\partial y}\right]. \tag{3.18b}$$

Consider now an integration of the continuity equation (3.17b) over the shaded area *S* shown in Fig. 5. This area consists of a simple rectangle enclosing the frontal jet, and, as mentioned, is characterized by having sides whose lengths are the intermediate length scale L_I. Upon substitution with (3.18a), the integration yields:

$$\underbrace{\iint_S \frac{\partial h}{\partial t}\,dxdy}_{(1)} - \underbrace{\iint_S \frac{1}{f}\nabla\times\left(\frac{g'h^2}{2}\mathbf{k}\right)dxdy}_{(2)} + \underbrace{\iint_S \nabla\cdot\left[\frac{\mathbf{k}\times\partial(h\mathbf{u})/\partial t}{f}\right]dxdy}_{(3)} + \underbrace{\oint_\phi \frac{1}{f}\mathbf{F}\cdot\mathbf{n}\,dl}_{(4)} = 0 \tag{3.19}$$

where $\mathbf{n}$ represents a unit vector pointing outward normal to the boundary of *S* (denoted by ϕ), and, as before, the Stokes theorem has been used so that *l* is an

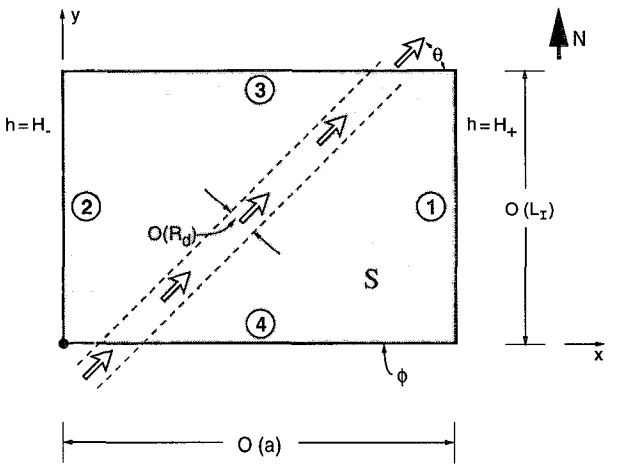

FIG. 5. A schematic diagram of a slanted jet. Dashed lines are contours of constant h. The quantity H_+ (H_-) denotes the undisturbed thickness in the far east (west) of the front. The angle θ measures inclination relative to north. L_I is any length scale that satisfies $R_d \ll L_I \ll a$ (where a is the radius of the earth) but, for convenience, we shall choose it to be the so-called intermediate length scale $f_0 R_d^2/\beta)^{1/3}$.

integration element along ϕ. Note that (3.19) is an exact statement given the reduced gravity equations.

Integral (2) of (3.19) yields

$$\iint \nabla\cdot\frac{1}{f}\left(\nabla\times\frac{g'h^2}{2}\hat{k}\right)dA = \equiv \int_1 \frac{\beta}{f^2}\frac{g'h^2}{2}\,dy - \int_2 \frac{\beta}{f^2}\frac{g'h^2}{2}\,dy, \quad (3.20)$$

where the numbers "1" and "2" denote the bounding sides of domain S indicated in Fig. 5. In the Appendix, it is demonstrated that integrals (3) and (4) in (3.19) are small compared to (1) and (2). The balance of (1) and (2) then yields

$$\iint \frac{\partial h}{\partial t}\,dxdy = \frac{\beta g'}{2f^2}(H_+^2 - H_-^2)L_I\left[1 + O\left(\frac{L_I}{a}\right)^2\right], \quad (3.21)$$

where, as mentioned, L_I is the intermediate length scale and a is the radius of the earth. If we now search for steadily propagating solutions, $\partial h/\partial t = -Ch_x$, the left-hand side of (3.21) becomes

$$\iint \frac{\partial h}{\partial t}\,dxdy = -C\int_1 h\,dy + C\int_2 h\,dy \approx -C[H_+ - H_-]L_I\left[1 + O\left(\frac{R_d}{a}\right)\right]$$

and we ultimately find our desired propagation rate:

$$C_x = -\frac{\beta g'}{f^2}\frac{(H_+ + H_-)}{2}(1 + O(R_d/a)), \quad (3.22)$$

which is identical to (3.16b).

Since the demonstration of the scaling leading to this result is algebraically tedious, the details are relegated to appendix A.

d. Discussion

The above analysis suggests fronts embedded between two large-scale water masses possess a β-driven propagation tendency whose magnitude is *independent* of the detailed structure of the front. Rather, the migration rate depends only upon the far-field structure away from the front. This dependence was implicit in the earlier analysis, where the fact that the integrals are dominated by these far-field contributions was used to arrive at (3.16).

Three points should be made about (3.22). First, it was not necessary here to assume that the front is nearly meridional and, therefore, it was not necessary to use an approximation like (3.4). Hence, we argue that the front propagation rate is largely insensitive to the jet's inclination. Second, (3.22) is identical to the reduced gravity limit of the shock propagation speed found in Dewar (1987). The analysis presented here, however, is considerably more general and supports the aptness of (3.22) for fronts regardless of the dynamics of their associated jet. [In comparison, the analysis in Dewar (1987) required the jet to be geostrophic.] Finally, we emphasize again the fundamental role placed by anisotropy in reducing (3.19) to (3.22). In a few words, the possible behaviors of a thermocline system constrained by anisotropy are such as to eliminate virtually any behavior other than migration at a speed controlled by β-plane geostrophic dynamics.

4. Application to the LDE jet

The two main components of the LDE experiment were the long-term moored array and the Intensive Hydrographic Program. The latter data are of more interest to the present discussion, and their analysis with respect to the LDE jet was discussed by Taft et al. (1986) and Shen et al. (1986). The history of the jet was that it appeared to form during the middle of the hydrographic program (between survey 3 and 4) at the center of the LDE region. The jet was subsequently observed until the final survey (survey 7), during which time it appeared to drift west at a speed between 3 and 5 km day^{-1} (3.5 to 5.6 cm s^{-1}). It also exhibited variability in amplitude and interacted with eddies, although these aspects of front behavior are not of central importance here.

A typical amplitude of the front, as measured by the cross-frontal change in depth of participating isopycnals, was on the order of 200 m. The hydrographic observations were also used to estimate the jet velocity field, and their analysis suggested the flows were surface intensified and caused a southwestward transport of 40 Sverdrups (Sv $\equiv 10^6$ m^3 s^{-1}).

We shall now argue that the previous analysis of jet drift on a β plane yields migration rates of the proper order to account for the LDE jet drift. To apply (3.16b), we need (in effect) an estimate of g'. Questions about applying a reduced gravity model to a continuously stratified ocean aside, this can essentially be obtained from the transport estimate. Approximating the along-jet speed v by geostrophy, the net jet transport can be expressed as

$$T = \int_{-\infty}^{\infty} vhdx = \int_{-\infty}^{\infty} \frac{\partial}{\partial x}\left(\frac{g'h^2}{2f}\right)dx$$

$$= \frac{g'}{2f}(H_+^2 - H_-^2).$$

Rewriting (3.16b) yields

$$C = -\left(\frac{\beta}{f}\frac{T}{(H_+ - H_-)}\right),$$

which upon use of the above observations yields

$$C = -\frac{2 \times 10^{-13}\ \text{cm}^{-1}\ \text{s}^{-1}}{10^{-4}\ \text{s}^{-1}} \times \frac{40 \times 10^{12}\ \text{cm}^3\ \text{s}^{-1}}{2 \times 10^4\ \text{cm}} = 4\ \text{cm s}^{-1}.$$

This compares favorably with the observed LDE jet drift of 3.5 to 5.6 cm s^{-1}.

In this context it should be pointed out that the Azores jet, which is also an elongated jet in the open ocean, seems to be in a quasi-permanent position. However, our analysis suggests that this jet should drift toward the western boundary. The apparent discrepancy between these two aspects can be reconciled by noting that the Azores jet is strongly affected by the local wind field (e.g., see Stramma and Siedler 1988) as well as a relatively strong mean flow (e.g., see Klein and Siedler 1989). These processes are almost certainly important in selecting preferred locations for the Azores jet.

5. Summary

This article introduces new aspects of nonlinear frontal jets; it focuses on topographically and β-induced drifts. Solutions have been constructed under the assumptions that (i) the ocean can be approximated by two layers, one of which can be taken to be at rest; (ii) the motion is approximately frictionless and nondiffusive; (iii) the jet has a cross-front length scale like the deformation radius and an alongfront scale that is considerably greater than this (here assumed to be the basin scale); and (iv) the jets translate without significant changes in their structure. The behavior of the jets can be summarized as follows.

1) Jets situated on a sloping bottom (Figs. 1, 2) translate along the isobaths with shallow water on their right-hand side (looking downstream in the Northern Hemisphere) at the *universal* speed $g'S/f_0$. The structure of the drifting jets is identical to the structure that they have over a *flat* bottom. All deep jets, regardless of their orientation, propagate in the same direction at the above-mentioned rate.

2) All upper-ocean jets, regardless of their orientation, propagate westward at the average of the two long planetary wave speeds appropriate to the two sides of the front, for example, $C = -[\beta(R_{d+}^2 + R_{d-}^2)/2]$, where $R_{d+}(R_{d-})$ is the deformation radius east (west) of the front. If the isopycnal surfaces, this simplifies to $C = -\beta R_d^2/2$, that is, half the long planetary wave speed. In contrast to deep jets, the structure of upper-ocean jets on a β plane differs at $O(\beta L/f_0)$ relative to their structure on an f plane. The detailed structure of the jets on the β plane is not found in this study, but it is expected that such jets will vary slowly in the downstream direction.

3) A fundamental difference between the drift of our midocean jets and the propagation of planetary waves is that jets carry mass with them as they propagate, whereas planetary waves are not necessarily associated with mass transport.

Application of the above theory to the jet observed during the LDE suggests that β-induced frontal migration can indeed account for the order of magnitude of the LDE jet drift. It is also interesting that jet migration rate (3.16) appears to be a very general formula and relatively independent of the jet dynamics.

On the other hand, it is worth making explicit a consideration present in reduced gravity β-plane dynamics that is not characteristic of the deep jet solution, and that represents a cautionary point regarding the LDE jet comparison. Specifically, β-induced steepening occurs in reduced gravity models mainly because thinner parts of the fluid move west more slowly than thicker parts. Therefore, shallow regions west of thick regions naturally form into fronts. The converse, however, is not true; thick regions west of shallow regions disperse in reduced gravity systems. The LDE jet falls into the latter category, suggesting that the application of reduced gravity dynamics for these data is perhaps questionable. On the other hand, the scaling leading to (3.22) is independent of questions regarding amplitude dispersion, and suggest only a bulk movement of an anisotropic thickness anomaly proportional to anomaly parameters. Hence, the average movement of the LDE front might well be related to the β-plane dynamics expressed in (3.22), even if all aspects of the motion are not accounted for in detail. Thus, we suggest β-induced migration as a possible explanation for the observed motion of the LDE jet.

Acknowledgments. This study was supported by National Science Foundation Grants OCE-9012114 and OCE-9102025, and by Office of Naval Research Grants N00014-89-J-1577 and N00014-89-J-1606. Drawings were prepared by Beth Raynor.

APPENDIX

Scale Analysis of (3.19)

a. Integral (4)

After some manipulation, this integral may be written as

$$\oint_\phi \frac{1}{f}\mathbf{F}\cdot\mathbf{n}\,dl = -\underline{\frac{1}{f}(vvh)_{1^+}} + \underline{\frac{1}{f}(vvh)_{1^-}} + \underline{\left(\frac{1}{f}vvh\right)_{2^+}} - \underline{\left(\frac{1}{f}vvh\right)_{2^-}} + \underline{\int_1 \frac{\beta}{f^2}vvhdy}$$

$$- \underline{\int_2 \frac{\beta}{f^2}vvhdy} - \underline{\int_1 \frac{(uvh)_x}{f}dy} + \underline{\int_2 \frac{(uvh)_x}{f}dy} + \underline{\frac{(uuh)_{3^+}}{f}} - \underline{\frac{(uuh)_{3^-}}{f}}$$

$$+ - \underline{\frac{(uuh)_{4^+}}{f}} + \underline{\frac{(uuh)_{4^-}}{f}} + \int_3 \frac{(uvh)_y}{f}dx - \int_4 \frac{(uvh)_y}{f}dx, \quad \text{(A.1)}$$

where 1^+ and 1^- denote the northern and southern ends of side 1. Similarly, 3^+ and 3^- denote the eastern and western ends of side 3.

The vertices of domain S have all been chosen to lie in the far field of the front, and are thus found in the sluggish, basin-scale water masses. To proceed with our analysis, we recall that in frontal geostrophic systems, velocity normally scales as $f_0R_d^2/L$. Furthermore, by noting that $f_0/\beta \sim O(a)$, we see that the far-field velocities should be scaled as $f_0R_d^2/a$, and, hence,

$$\frac{(uuh)}{f}4_+ = O\left(\frac{f_0^2R_d^4H_1}{a^2f_0}\right) = O\left[\beta H_1R_d^2L_I\left(\frac{L_I}{a}\right)^2\right] \quad \text{(A.2)}$$

(where H_1 is the larger of H_+ and H_-), which is obviously considerably smaller than the result quoted in (3.21). Other quantities in (A.1), such as

$$\int_1 \frac{\beta}{f^2}(vvh)dy,$$

involve integrations entirely through large-scale zones, and thus scale according to

$$\int_1 \frac{\beta}{f^2}(vvh)dy = O\left(\frac{\beta}{f_0^2}\frac{f_0^2R_d^4}{a^2}H_1L_I\right)$$

$$= O(\beta H_1R_d^2)L_I\left(\frac{R_d^2}{a^2}\right) \quad \text{(A.3)}$$

and are similarly negligible compared to (3.21). Finally, quantities like

$$\int_1 \frac{\partial(uvh)/\partial x}{f}dy$$

scale as

$$\int_1 \frac{\partial(uvh)/\partial x}{f}dy = O\left(\frac{f_0R_d^4L_IH_1}{a^3}\right)$$

$$= O\left[\beta R_d^2H_1L_I\left(\frac{L_I}{a}\right)^3\right] \quad \text{(A.4)}$$

for similar reasons.

All underlined terms in (A.1) may thus be neglected relative to integral (2) in (3.19), which thus reduces to the approximate statement:

$$\int\int \frac{\partial h}{\partial t}dxdy + \int\int \nabla\frac{\mathbf{k}\times\partial(h\mathbf{u})/\partial t}{f}dxdy - \int_1 \frac{\beta}{f^2}\frac{g'h^2}{2}dy + \int_2 \frac{\beta}{f^2}\frac{g'h^2}{2}dy$$

$$+ \int_3 \frac{\partial(uvh)/\partial y}{f}dx - \int_4 \frac{\partial(uvh)/\partial y}{f}dx = O\left[\beta H_1R_d^2L_I\left(\frac{L_I}{a}\right)^2\right]. \quad \text{(A.5)}$$

b. Integral (3)

Integral (3) can be rewritten as:

$$\int\int \nabla\cdot\left(\frac{\mathbf{k}\times\partial(h\mathbf{u})/\partial t}{f}\right)dxdy = -\int_1 \frac{\partial(hv)/\partial t}{f}dy + \int_2 \frac{\partial(hv)\partial t}{f}dy + \int_3 \frac{\partial(hu)/\partial t}{f}dx - \int_4 \frac{\partial(hu)/\partial t}{f}dx. \quad \text{(A.6)}$$

Estimation of (A.6) requires a time scale, and two apply to the present problem. The less interesting one is f_0^{-1}, and is associated with gravity wave activity. We are interested in the front influence forced by β, in which case time scales as $(\beta R_d)^{-1}$. Thus, the first two terms in (A.6), which are integrals entirely through large-scale zones, scale as:

$$\int_1 \frac{\partial(hv)/\partial t}{f}\,dy = \mathrm{O}\left(H_1 \frac{f_0 R_d^2 \beta R_d}{a f_0} L_I\right) = \mathrm{O}\left[\beta R_d^2 H_1 L_I\left(\frac{R_d}{a}\right)\right],$$

which is small relative to the retained terms in (A.5).

Further, given that the far-field length scale a is large compared to L_I, which is the scale over which the integrals are performed,

$$\int_1 \frac{\beta}{f^2}\frac{g'h^2}{2}\,dy = \frac{g'}{2}\int\left[\frac{\beta h^2}{f^2}(y_0) + \left(\frac{\beta h^2}{f^2}\right)_y (y - y_0)\right]dy = \frac{g'\beta h^2(y_0) L_I}{2f^2}\left[1 + \mathrm{O}\left(\frac{L_I}{a}\right)^2\right],$$

where y_0 is a central latitude point within S. Gathering the above, (A.5) is reduced to

$$\iint \frac{\partial h}{\partial t}\,dxdy + \int_S\int \frac{\partial}{\partial y}\left(\frac{\partial(hu)/\partial t}{f}\right)dS - \frac{\beta g'}{2f^2}(H_+^2 - H_-^2)L_I + \int_3 \frac{\partial(uvh)/\partial y}{f}\,dx - \int_4 \frac{\partial(uvh)/\partial y}{f}\,dx = \mathrm{O}\left[\beta H_1 R_d^2 L_I\left(\frac{R_d}{a}\right)\right], \quad \text{(A.7)}$$

where the notation H_+ has been used for $h(y_0)$ east of the front and H_- for $h(y_0)$ west of the front.

c. *Cross-jet integrals*

Consider some arbitrary property of the front q. This may be, for example, h, v, u, or any combination of these variables. In the vicinity of the front, the gradient of q occurs dominantly across the front on a scale of the deformation radius and generally involves the full order of magnitude of the quantity q. For example, if $q = u$,

$$\nabla u \approx \mathrm{O}\left(\frac{f_0 R_d}{R_d}\right)\hat{\mathbf{n}},$$

where $\hat{\mathbf{n}}$ is the unit normal vector to the front. In contrast, the anisotropy of the front insures that tangential gradients are much smaller, that is,

$$\nabla \mathbf{u}\cdot\mathbf{t} = \mathrm{O}\left(f_0 \frac{R_d}{a}\right),$$

where $\mathbf{t}$ is a tangential unit vector to the front.

Consider then, as an example, the quantity $\nabla(huv)$. In Cartesian coordinates, this is $\nabla(huv) = \partial(huv)/\partial x\hat{\mathbf{x}} + \partial(huv)/\partial y\hat{\mathbf{y}}$. Normal and tangent vectors to the front can be calculated from the gradients of h; that is,

$$\mathbf{n} = \frac{\left(\frac{\partial h}{\partial x}, \frac{\partial h}{\partial y}\right)}{|\nabla h|}; \quad \mathbf{t} = \frac{\left(\frac{-\partial h}{\partial y}, \frac{\partial h}{\partial x}\right)}{|\nabla h|}. \quad \text{(A.8)}$$

Inverting (A.8) yields

$$\frac{\left(\frac{\partial h}{\partial x}\mathbf{n} - \frac{\partial h}{\partial y}\mathbf{t}\right)}{|\nabla h|} = \mathbf{x} \qquad \frac{\left(\frac{\partial h}{\partial y}\mathbf{n} + \frac{\partial h}{\partial x}\mathbf{t}\right)}{|\nabla h|} = \mathbf{y}.$$

Therefore,

$$\nabla(huv) = \frac{[\partial/\partial x(huv)\partial h/\partial x + \partial/\partial y(huv)\partial h/\partial y]}{|\nabla h|}\mathbf{n} + \frac{[\partial/\partial y(huv)\partial h/\partial x - \partial/\partial x(huv)\partial h/\partial y]}{|\nabla h|}\mathbf{t}. \quad \text{(A.9)}$$

The weakness of the tangential gradient insures that

$$\frac{\partial(huv)}{\partial y} = \frac{\partial(huv)}{\partial x}\frac{\partial h}{\partial y}\Big/\frac{\partial h}{\partial x}\left[1 + \mathrm{O}\left(\frac{R_d}{a}\right)\right] = \frac{-\partial(huv)}{\partial x}\frac{\partial x}{\partial y}\Big|_h\left[1 + \mathrm{O}\left(\frac{R_d}{a}\right)\right], \quad \text{(A.10)}$$

where the differential $\partial x/\partial y$ is taken along a line of constant h.

From Fig. 5, it is seen that $\partial x/\partial y = \tan\theta$, where θ is the angle between h contours and true north. Further, the anisotropy of the front insures us that variations of θ are "slow" and occur on the "a" length scale. The usefulness of the above results [(A.10) in particular] comes in evaluating integrals in (A.7) through the front. Consider, for example,

$$\int_3 \frac{\partial(uvh)/\partial y}{f}\,dx,$$

which is one integral to which this analysis applies. The subscript 3 denotes the side of the integration domain on which the integration is performed. According to the above analysis,

$$\int_3 \frac{\partial(uvh)/\partial y}{f}\,dx = -\frac{1}{f}\int_3 \frac{\partial(huv)/\partial x}{f}\tan\theta dx$$

$$= -\frac{\tan\theta}{f}\left[(huv)_{3_+} - (huv)_{3_-}\right], \quad \text{(A.11)}$$

and thus the integral may be equated to far-field terms whose order of magnitude can be deduced from the previous scaling. The order of these terms is given by

$$\frac{huv}{f} = \mathrm{O}\left[H_1\frac{f_0^2R_d^4}{f_0a^2}\right] = \mathrm{O}\left[\beta H_1 R_d^2 L_I\left(\frac{L_I}{a}\right)^2\right].$$

Similar arguments apply to terms in (A.7) such as

$$\int\int \frac{\partial}{\partial y}\left(\frac{\partial(hu)/\partial t}{f}\right)dxdy = -\frac{\tan\theta}{f}\int_1 \frac{\partial}{\partial t}(hu)dy$$

$$+\frac{\tan\theta}{f}\int_2 \frac{\partial}{\partial t}(hu)dy. \quad \text{(A.12)}$$

Time scales in the geostrophic far field behave like $(\beta R_d)^{-1}$, so that the above scale is

$$\frac{\tan\theta}{f}\int_1 \frac{\partial}{\partial t}(hu)dy \approx \frac{1}{f_0}H_1\frac{f_0R_d^2}{a}\beta R_d L_I$$

$$= \mathrm{O}\left[\beta H_1 R_d^2 L_I\left(\frac{R_d}{a}\right)\right].$$

This completes the estimation of all the terms in the equation; collecting all the results (A.7) reduces to (3.21) as stated earlier.

REFERENCES

Dewar, W. K., 1987: Planetary shock waves. *J. Phys. Oceanogr.*, **17,** 470–482.

——, 1991: Arrested fronts. *J. Mar. Res.*, **49,** 21–52.

——, and J. C. Marshall, 1993: Inertial embedded fronts. *J. Phys. Oceanogr.*, in press.

Gill, A. E., 1982: *Atmospheric-Ocean Dynamics.* Academic Press, 662 pp.

Klein, B., and G. Siedler, 1989: On the origin of the Azores Current. *J. Geophys. Res.*, **94,** 6159–6168.

Mory, M., 1985: Integral constraints on bottom and surface isolated eddies. *J. Phys. Oceanogr.*, **15,** 1433–1438.

——, M. E. Stern, and R. W. Griffiths, 1987: Coherent baroclinic eddies on a sloping bottom. *J. Fluid Mech.*, **183,** 45–62.

Nof, D., 1983a: On the migration of isolated eddies with application to Gulf Stream rings. *J. Mar. Res.*, **41,** 399–425.

——, 1983b: The translation of isolated cold eddies on a sloping bottom. *Deep-Sea Res.*, **30,** 171–182.

Shen, C., J. C. McWilliams, B. A. Taft, C. Ebbesmeyer, and E. J. Lindstrom, 1986: The mesoscale spatial structure and evolution of dynamical and scalar properties observed in the Northwestern Atlantic Ocean during the POLYMODE Local Dynamics Experiment. *J. Phys. Oceanogr.*, **16,** 454–482.

Stramma, L., and G. Siedler, 1988: Seasonal changes in the North Atlantic Subtropical gyre. *J. Geophys. Res.*, **93,** 8111–8118.

Swaters, G. E., and G. Flierl, 1991: Dynamics of ventilated coherent cold eddies on a sloping bottom. *J. Fluid Mech.*, **223,** 565–587.

Taft, B., E. J. Lindstrom, C. Ebbesmeyer, C. Y. Shen, and J. C. McWilliams, 1986: Water mass structure during the POLYMODE Local Dynamics Experiment. *J. Phys. Oceanogr.*, **16,** 403–426.